Journal of Polymers and the Environment (2021) 29:2855–2868
https://doi.org/10.1007/s10924-021-02057-x

ORIGINAL PAPER

# Fabrication of Schiff's Base Chitosan-Glutaraldehyde/Activated Charcoal Composite for Cationic Dye Removal: Optimization Using Response Surface Methodology

**Ali H. Jawad[1] · Ahmed Saud Abdulhameed[2] · Lee D. Wilson[3] · M. A. K. M. Hanafiah[4] · W. I. Nawawi[5] · Zeid A. ALOthman[6] · Mohammad Rizwan Khan[6]**

Accepted: 11 January 2021 / Published online: 11 February 2021


## Abstract

In this work, a ternary composite containing a Schiff base adduct (chitosan-glutaraldehyde) along with activated charcoal (Ch-Glu/AC) was successfully prepared that contains activated charcoal with cross-linked chitosan. The Schiff base adduct was obtained by reaction of a dialdehyde bifunctional cross-linker agent (glutaraldehyde; Glu), where various methods were employed to study the morphology, material crystallinity, surface area, and surface functional group of the ternary composite (Ch-Glu/AC). Ch-Glu/AC was applied as an adsorbent to remove a cationic dye (thionine dye, TH) from aqueous media. The effect of various independent variables on the adsorption process including adsorbent dose (A: 0.02–0.1 g), solution pH (B: 4–10), temperature (C: 30–50 °C), and time (D: 30–180 min) were investigated and optimized using response surface methodology-Box–Behnken design (RSM-BBD). The results demonstrated that TH dye adsorption on the Ch-Glu/AC surface obeyed the pseudo-first order (PFO) kinetic model, and the Freundlich isotherm was obeyed at equilibrium. The maximum adsorption capacity ($q_m$) of the TH dye was 30.8 mg/g at 50 °C. The TH dye adsorption mechanism onto the composite surface was attributed to the electrostatic interaction, π-π interaction, and H-bonding. The findings of this work reveal the feasibility of Ch-Glu/AC as a candidate adsorbent for effective removal of cationic dyes from aquatic media.

**Keywords** Chitosan · Glutaraldehyde · Activated charcoal · Adsorption · Thionine dye · Box–behnken design

## Introduction

Many industries such as leather, paper, cosmetics, plastics, pharmaceuticals, and textile utilize cationic dyes like thionine (TH) for coloring of fabricated items [1]. The release of these colorants into water bodies is known to have detrimental consequences for humans and ecosystems [2]. Therefore, the removal of colorants prior to release of treated wastewater into water bodies is necessary precautionary measure. Various treatment methods have been applied to treat dyes from contaminated water such as electrochemical advanced oxidation [3], photodegradation [4], ion exchange [5], adsorption [6], and coagulation-flocculation [7]. Among these methods, adsorption is one of the most promising treatment strategies because of its facile operation, low-sensitivity to variable contaminations, low cost, adsorbent regeneration, high effectiveness, and high efficiency [8, 9]. Chitosan (Ch) is a cationic biopolymer that contains units of β-(1–4) acetyl-D-glucosamine. Ch can be produced commercially from chitin obtained from various sources such as s

✉ Ali H. Jawad
ali288@uitm.edu.my; ahjm72@gmail.com

1 Faculty of Applied Sciences, Universiti Teknologi MARA, 40450 Shah Alam, Selangor, Malaysia

2 Department of Medical Instrumentation Engineering, Al-Mansour University College, Baghdad, Iraq

3 Department of Chemistry, University of Saskatchewan, Saskatoon, SK S7N 5C9, Canada

4 Faculty of Applied Sciences, Universiti Teknologi MARA, 26400 Jengka, Pahang, Malaysia

5 Faculty of Applied Sciences, Universiti Teknologi MARA, 02600 Arau, Perlis, Malaysia

6 Chemistry Department, College of Science, King Saud University, 11451 Riyadh, Saudi Arabia

shrimp, lobster and crabs, algae, and fungi by chemical deacetylation of chitin [10, 11]. Ch has remarkable properties such as biodegradability, chemical reactivity, non-toxicity, biocompatibility, hydrophilicity, adsorption ability, chelation, and anti-bacterial activity [12]. Furthermore, Ch has outstanding functional groups (amine and hydroxyl), which can be adopted for the adsorption of metal ions [13] and dye species [14]. In general, the application of Ch (unmodified form) to adsorption processes are finite because of its leaching potential, solubility in acidic media, and high swelling index [15]. Hence, it is of great significance to modify Ch to improve its adsorptive property, biopolymer surface area and chemical stability. Various methods have been applied to enhance the physiochemical properties of Ch by cross-linking and composite formation with carbonaceous materials such as activated carbon [16, 17]. Cross-linking reaction of Ch is a convenient approach for modifying the stability of Ch in acidic media and enhancing its mechanical strength, in addition to alteration of the biopolymer hydrophobicity [18]. Generally, activated charcoal is a porous carbonaceous network material that consists of carbon in a quasi-graphitic form [19]. AC offers several desirable features when it is utilized as an adsorbent due to its extensive surface area and porous structure [20]. Recently, Ch-AC composites have been utilized in several applications such as removal of dyes [13], metal ions [21], and antibiotics [22], along with other applications such as hydrogen storage [23], $CO_2$ capture [24], antibacterial activity [25], and catalysts [26].

Naturally, Ch is a cationic biopolymer with high affinity to adsorb anionic dyes from aqueous solutions, especially after protonating its amine ($–NH_3^+$) groups in acidic environments. According to a survey of the literature, there are no comprehensive studies on the removal of cationic dyes by Ch and/or its composite forms. Therefore, the main objective of the current research is to develop a composite synthetic Schiff's base chitosan-glutaraldehyde/activated charcoal (Ch-Glu/AC) as a chemically stable adsorbent material for the effective removal of cationic species from aqueous solution. Thus, this ternary composite was prepared by loading AC powder into polymeric matrix of Ch, followed by a Schiff's base cross-linking step using glutaraldehyde (Glu). The effectiveness of the composite Ch-Glu/AC was evaluated for removal of a model cationic dye thionine (TH) from aqueous solution. A response surface methodology-Box-Behnken design (RSM-BBD) was utilized in this study for optimizing the key adsorption parameters such as adsorbent dose, solution pH, temperature, and contact time. The adsorption kinetics, equilibrium adsorption isotherms, and mechanism of TH dye uptake was investigated.

## Materials and Methods

### Materials

Ch (deacetylation ≥ 75%; medium molecular weight), aqueous glutaraldehyde (Glu) solution (50%) were obtained from Sigma–Aldrich. Activated charcoal (AC) powder with particle size (< 100 µm) was purchased from Merck, Germany. TH dye (MW: 319.86 g/mol, $\lambda_{max} = 569$ nm, assay: 99%), potassium hydroxide (KOH), hydrochloric acid (HCl) were obtained from R&M Chemicals.

### Preparation of Ch-Glu/AC

The Ch-Glu/AC was produced by adding 2 g of Ch and AC (1:1) to solution of acetic acid (5% v/v, 50 mL) with vigorous stirring for 24 h at 27 °C to dissolve the Ch flakes. The viscous solution of Ch/AC was injected to solution of NaOH (0.5 M, 1000 mL) using a syringe needle (10 mL) to form beads of Ch/AC. The Ch/AC beads were washed with deionized water for removing NaOH residual. The crosslinking reaction was implemented by adding of 1% Glu (90 mL) to the Ch/AC beads under slow shaking in water bath at 40 °C for 2 h. Subsequently, the washing of the manufactured beads (Ch-Glu/AC) was performed with deionized water, followed by oven drying for 24 h along with sample crushing. Eventually, the Ch-Glu/AC sample was ground to get a powder (size ≤ 250 µm) for experiments of TH adsorption.

### Characterization

Micromeritics ASAP 2060 analyzer was used for measuring the specific surface area of Ch-Glu/AC using $N_2$ adsorption/desorption isotherms at 77 K. Scanning electron microscopy-energy dispersive X-ray (SEM–EDX, Zeiss Supra 40 VP) was used for analysis of the morphology of Ch-Glu/AC and Ch-Glu/AC after TH dye uptake. X-ray diffractometer (XRD, X'Pert PRO, PAnalytical) was used for the determining structure nature of Ch-Glu/AC. The zero point of charge ($pH_{pzc}$) measure was performed for determining surface charge of the Ch-Glu/AC as described in the literature [27]. Fourier transform infrared (FTIR) spectroscopy (Perkin-Elmer, Spectrum RX I) was used for the determining the functional groups on the surface of the Ch-Glu/AC before and after TH dye uptake.

### Experimental Design

In this study, RSM-BBD was applied for optimization of the impacts of four factors: adsorbent dose, pH, temperature, and time on the TH dye adsorption by Ch-Glu/AC. The Design Expert 11.0 (Stat-Ease, Minneapolis, USA) software

**Table 1** Codes and actual ranges of independent variables and their levels

| Codes | Variables | Level 1 (− 1) | Level 2 (0) | Level 3 (+ 1) |
|---|---|---|---|---|
| A | Adsorbent dose (g) | 0.02 | 0.06 | 0.1 |
| B | Solution pH | 4 | 7 | 10 |
| C | Temperature (℃) | 30 | 40 | 50 |
| D | Time (min) | 30 | 105 | 180 |

was used for designing adsorption tests and statistical analysis of the experimental data. Table 1 lists the levels of factors utilized in the BBD model. A quadratic equation was used for predicting the dye removal efficiency and analysis of experimental result, as follows (1):

$$Y = \beta_0 + \sum \beta_i X_i + \sum \beta_{ii} X_i^2 + \sum \sum \beta_{ij} X_i X_j \quad (1)$$

where $Y$ is the predicted response for TH dye removal (%); $X_i$ and $X_j$ are coded as the independent variables; $\beta_0$ is the constant; $\beta_i$, $\beta_{ii}$ and $\beta_{ij}$ are coefficients of linear, quadratic, and interactive coefficient of factors, respectively. Generally, 29 runs were generated from the BBD model to optimize the four factors (A: adsorbent dose of 0.02–0.1 g, B: pH of 4–10, C: temperature of 30–50 °C and D: time of 30–180 min) on the TH dye removal (%) by the adsorbent. The BBD matrix and the results of response (TH dye removal, %) are listed in Table 2. A specified quantity of adsorbent was taken in a set of Erlenmeyer flasks (250 mL) containing a dye solution (100 mL). These flasks were held in a water bath (WNB7-45, Memmert, Germany) and shaken at 100 rpm. Then, the adsorbents were removed from the TH dye solutions by syringe filter (0.45 µm). The initial and final of TH concentrations were measured by UV–Vis spectroscopy (HACH DR 2800) at the $\lambda_{max} = 569$ nm. The TH dye removal (DR %) was calculated by Eq. 2.

$$DR(\%) = \frac{(C_o - C_e)}{C_o} \times 100\% \quad (2)$$

where $C_o$ (mg/L) and $C_e$ (mg/L) are the initial and final TH dye concentration, respectively.

## Adsorption Study of TH on Ch-Glu/AC

The uptake of TH dye by Ch-Glu/AC was investigated by the batch approach. Based on Table 2 (specifically run 16), the optimum conditions for the highest TH dye removal (%) occurred at an adsorbent dose of 0.06 g, pH 10, and 50 °C. Thus, the adsorption experiments were carried out with these conditions at variable initial dye concentration (10–100 mg/L) and variable contact time (0–360 min). The TH dye adsorption experiments were done by following the same procedure outlined above. The adsorption capacity of Ch-Glu/AC toward TH dye at equilibrium, $q_e$ (mg/g) was calculated by Eq. (3):

$$q_e = \frac{(C_o - C_e)V}{W} \quad (3)$$

where $V$ (L) and $W$ (g) represent the volume of TH solution and mass of Ch-Glu/AC, respectively.

**Table 2** The 4-varibles BBD matrix and experimental data for TH dye removal

| Run | A:Adsorbent dose (g) | B:pH | C:Temp (°C) | D:Time (min) | TH removal (%) |
|---|---|---|---|---|---|
| 1 | 0.02 | 4 | 40 | 105 | 7.5 |
| 2 | 0.1 | 4 | 40 | 105 | 35.2 |
| 3 | 0.02 | 10 | 40 | 105 | 43.7 |
| 4 | 0.1 | 10 | 40 | 105 | 49.7 |
| 5 | 0.06 | 7 | 30 | 30 | 15.5 |
| 6 | 0.06 | 7 | 50 | 30 | 28.0 |
| 7 | 0.06 | 7 | 30 | 180 | 14.0 |
| 8 | 0.06 | 7 | 50 | 180 | 19.9 |
| 9 | 0.02 | 7 | 40 | 30 | 11.4 |
| 10 | 0.1 | 7 | 40 | 30 | 40.0 |
| 11 | 0.02 | 7 | 40 | 180 | 16.3 |
| 12 | 0.1 | 7 | 40 | 180 | 25.5 |
| 13 | 0.06 | 4 | 30 | 105 | 3.88 |
| 14 | 0.06 | 10 | 30 | 105 | 25.4 |
| 15 | 0.06 | 4 | 50 | 105 | 15.3 |
| 16 | 0.06 | 10 | 50 | 105 | 59.2 |
| 17 | 0.02 | 7 | 30 | 105 | 15.4 |
| 18 | 0.1 | 7 | 30 | 105 | 21.3 |
| 19 | 0.02 | 7 | 50 | 105 | 17.5 |
| 20 | 0.1 | 7 | 50 | 105 | 33.0 |
| 21 | 0.06 | 4 | 40 | 30 | 8.56 |
| 22 | 0.06 | 10 | 40 | 30 | 43.8 |
| 23 | 0.06 | 4 | 40 | 180 | 9.70 |
| 24 | 0.06 | 10 | 40 | 180 | 35.0 |
| 25 | 0.06 | 7 | 40 | 105 | 20.5 |
| 26 | 0.06 | 7 | 40 | 105 | 25.9 |
| 27 | 0.06 | 7 | 40 | 105 | 22.3 |
| 28 | 0.06 | 7 | 40 | 105 | 21.4 |
| 29 | 0.06 | 7 | 40 | 105 | 24.7 |

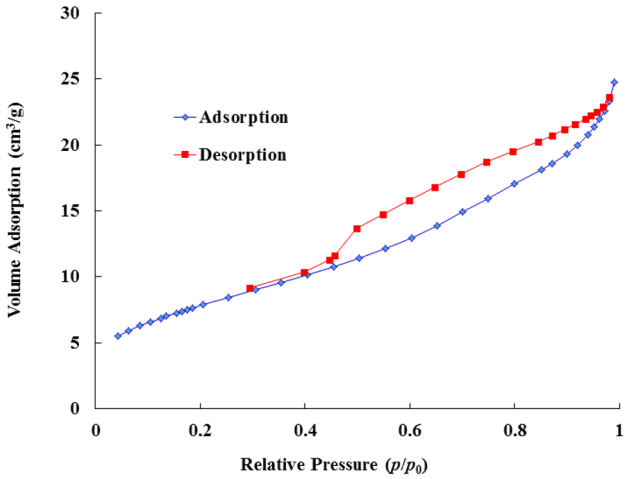


**Fig. 1** $N_2$ adsorption–desorption isotherms of Ch-Glu/AC composite

**Table 3** Textural properties of Ch-Glu/AC composite

| Property | Value |
|---|---|
| $V_m$ ($cm^3$ /g) | 6.49 |
| Total pore volume ($cm^3$/g) | 0.04 |
| BET surface area ($m^2$/g) | 28.3 |
| Mean pore diameter (nm) | 5.38 |

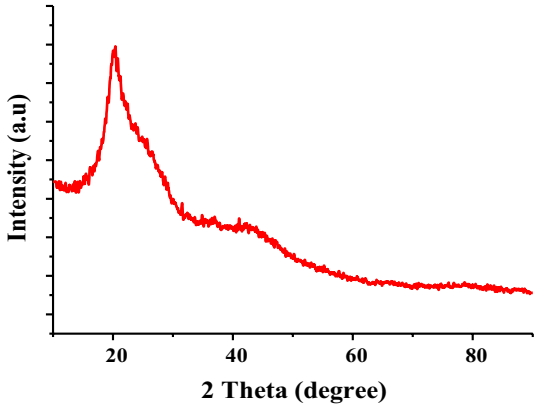


**Fig. 2** XRD profile of the Ch-Glu/AC composite

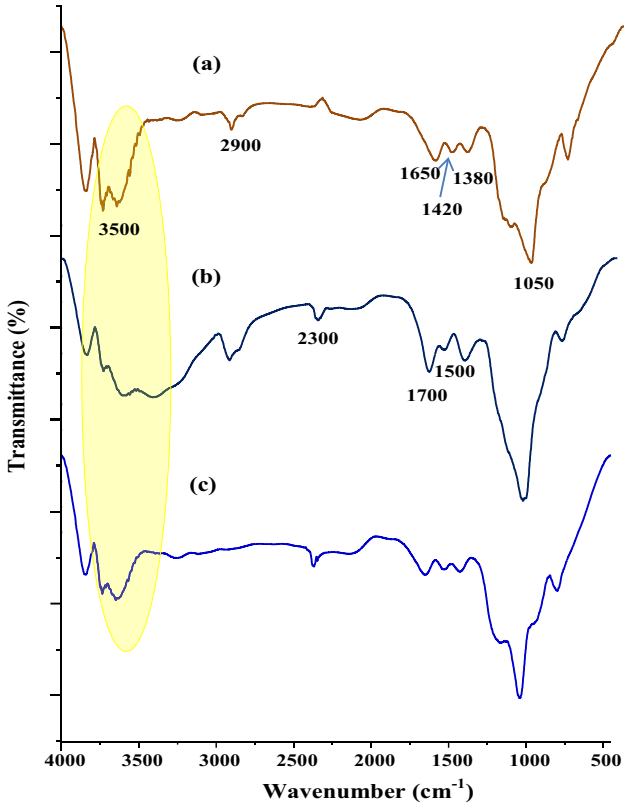


**Fig. 3** FTIR spectra of (a) Ch-Glu, (b) Ch-Glu/AC composite, and (c) Ch-Glu/AC composite after adsorption of the TH dye

## Results and Discussion

### Characterization of the Ch-Glu/AC Composite

The specific surface area and porous structure of Ch-Glu/AC was characterized by $N_2$ adsorption/desorption isotherms as shown in Fig. 1. According to the IUPAC classification, the $N_2$ physisorption isotherm was consistent with type IV behavior, indicating the existence of mesoporosity in the composite structure of Ch-Glu/AC. The surface properties of the Ch-Glu/AC composite are listed in Table 3, where the ternary composite has a mean pore diameter of 5.38 nm, further confirming that the Ch-Glu/AC composite has mesoporous structure [28]. Hence, the pore structure of Ch-Glu/AC signifies a mesoporous material with an increase of ca. 76.4 times (BET SA = 28.3 $m^2$/g) as compared with Ch-Glu before addition of AC (BET SA = 0.37 $m^2$/g), as reported in a previous study [29]. Thus, the surface area and mesopores of Ch-Glu/AC may contribute for enhancing the uptake of TH molecules on the surface of the Ch-Glu/AC composite and diffusion of TH molecules in the pores of the composite adsorbent.

The XRD pattern of the Ch-Glu/AC is shown in Fig. 2, where characteristic diffraction signatures occur at 2θ values 24° and 42°, which correspond to the (002) and (100), respectively. These XRD lines indicate that the Ch-Glu/AC structure is amorphous and also contains graphite crystallites from the AC fraction [29, 30].

FTIR spectra of Ch-Glu, Ch-Glu/AC, Ch-Glu/AC after dye uptake are shown in Fig. 3a–c. The IR spectrum of Ch-Glu (Fig. 3a) presents characteristic peaks which are

assigned, as follows: 3500 $cm^{-1}$ (hydroxyl –OH stretching vibrations), 2900 $cm^{-1}$ (C–H stretching vibration), 1650 $cm^{-1}$ (amide bond C=N stretching vibration), 1380 $cm^{-1}$ (C–O stretching vibration), 1380 $cm^{-1}$ (C–N stretching vibration), and 1050 $cm^{-1}$ (C–O–C vibration) [15, 23]. The IR spectrum of Ch-Glu/AC (Fig. 3b) shows significant changes, particularly the peak intensity of -OH over the 3500–3300 $cm^{-1}$ range, where the IR band is notably shifted, broadened and attenuated. This observation indicates hydrogen bonding between AC and Ch-Glu. Furthermore, IR spectrum of Ch-Glu/AC shows bands at 2300 $cm^{-1}$, 1700 $cm^{-1}$, and 1500 $cm^{-1}$, which are assigned to C≡C stretching vibration, carbonyl C=O stretching vibration, and C=C stretching vibration, respectively [21, 23]. The IR spectrum of the Ch-Glu/AC (Fig. 3c) after TH dye adsorption shows a similar profile to Ch-Glu/AC with a slight shifting in some bands that indicate the functional groups of the Ch-Glu/AC are involved in the adsorption process of TH dye.

SEM–EDX analysis was used to study the morphology of Ch-Glu/AC, before and after TH dye uptake, as illustrated in Fig. 4a and b. In Fig. 4a, it is evident that the surface morphology of Ch-Glu/AC contains textural porosity, along with the presence of cracks and crevices. The mesoporous structure of the Ch-Glu/AC is a favourable adsorbent that displays efficient adsorption of organics such as the TH dye. The EDX analysis reveals the presence of C, O, and N in the composite structure of Ch-Glu/AC. After uptake of the TH dye, the surface morphology of Ch-Glu/AC (Fig. 4b) becomes more compact with a reduced textural porosity that indicates TH dye uptake occurs onto the Ch-Glu/AC surface. The EDX analysis displays the existence of S which also supports the adsorption of TH dye on the surface of Ch-Glu/AC.

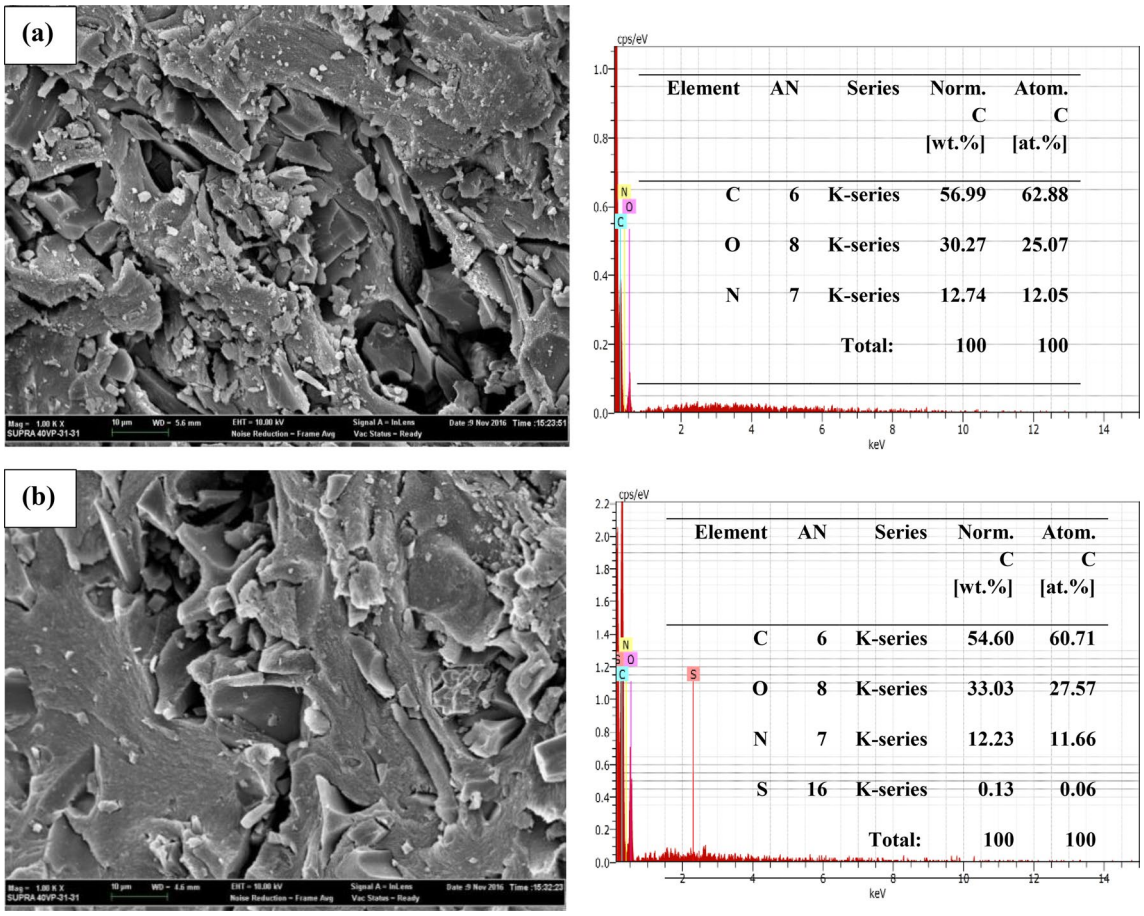


**Fig. 4** SEM–EDX analysis of **a** Ch-Glu/AC composite, and **b** Ch-Glu/AC composite after adsorption of the TH dye

**Table 4** Analysis of variance (ANOVA) for the removal of TH dye by Ch-Glu/AC composite

| Source | Sum of squares | df | Mean Square | F-value | p-value |
|---|---|---|---|---|---|
| Model | 4748.71 | 14 | 339.19 | 16.72 | < 0.0001 |
| A-Adsorbent dose | 716.89 | 1 | 716.89 | 35.33 | < 0.0001 |
| B-pH | 2601.75 | 1 | 2601.75 | 128.23 | < 0.0001 |
| C-Temperature | 501.84 | 1 | 501.84 | 24.73 | 0.0002 |
| D-Time | 60.41 | 1 | 60.41 | 2.98 | 0.1064 |
| AB | 117.21 | 1 | 117.21 | 5.78 | 0.0307 |
| AC | 23.09 | 1 | 23.09 | 1.14 | 0.3042 |
| AD | 94.43 | 1 | 94.43 | 4.65 | 0.0488 |
| BC | 124.65 | 1 | 124.65 | 6.14 | 0.0265 |
| BD | 24.93 | 1 | 24.93 | 1.23 | 0.2864 |
| CD | 11.02 | 1 | 11.02 | 0.5432 | 0.4733 |
| $A^2$ | 71.98 | 1 | 71.98 | 3.55 | 0.0806 |
| $B^2$ | 224.32 | 1 | 224.32 | 11.06 | 0.0050 |
| $C^2$ | 47.16 | 1 | 47.16 | 2.32 | 0.1496 |
| $D^2$ | 50.51 | 1 | 50.51 | 2.49 | 0.1369 |
| Residual | 284.05 | 14 | 20.29 | | |
| Lack of Fit | 263.46 | 10 | 26.35 | 5.12 | 0.0648 |
| Cor Total | 5032.76 | 28 | | | |

## BBD Model Analysis

The experimental results of the removal TH dye were statistically evaluated through analysis of variance (ANOVA) as presented in Table 4. Accordingly, the F-value of the BBD model was 18.26 with a corresponding p-value of (< 0.0001). This result reveals the statistical significance of the BBD model for removal of the TH dye [31]. The good agreement between actual and expected of TH dye removal values is concluded from the coefficient of determination ($R^2 = 0.94$). Statistically, any term of BBD model has a p-value < 0.05 is significant. Therefore, the terms of the model including A, B, C, $B^2$, AB, AD, and BC are significant in the removal of the TH dye. The other terms of coded factors with p-value > 0.05 are eliminated in the model equation to obtain the most reliable estimates using the model. The relationship between studied factors and the TH dye removal (response) is achieved by a second-order polynomial Eq. 4 as follows:

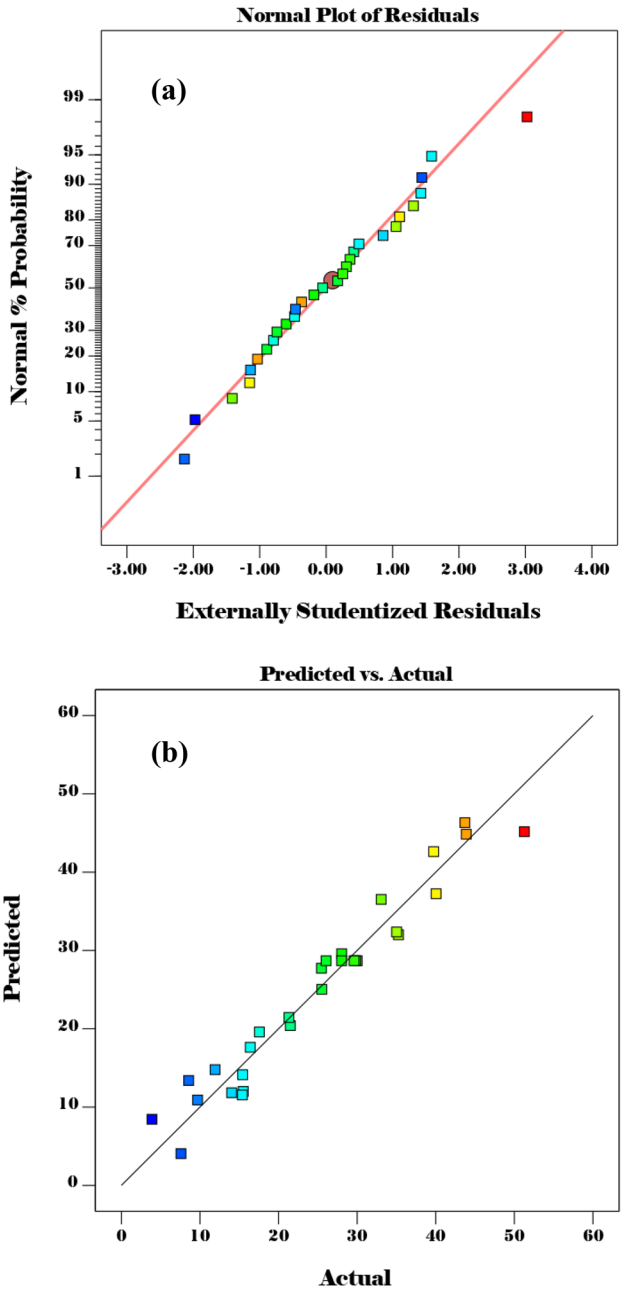


**Fig. 5** **a** Normal probability plot of residuals for TH dye removal, **b** plot of the relationship between the predicted and actual values of TH removal (%)

$$\text{TH removal } (\%) = +22.96 + 7.73A + 14.72B + 6.47C - 5.41AB - 4.86AD + 5.58BC + 5.88B^2 \quad (4)$$

The normal probability of the residuals can be seen in Fig. 5a, where the points reveal a linear trend line, indicating the ideal normal distributions of the residuals [32]. Figure 5b presents the relationship between the actual and expected TH dye removal values. The statistical goodness-of-fit by the BBD model can be concluded from Fig. 5b, where the actual and expected values are closely aligned.

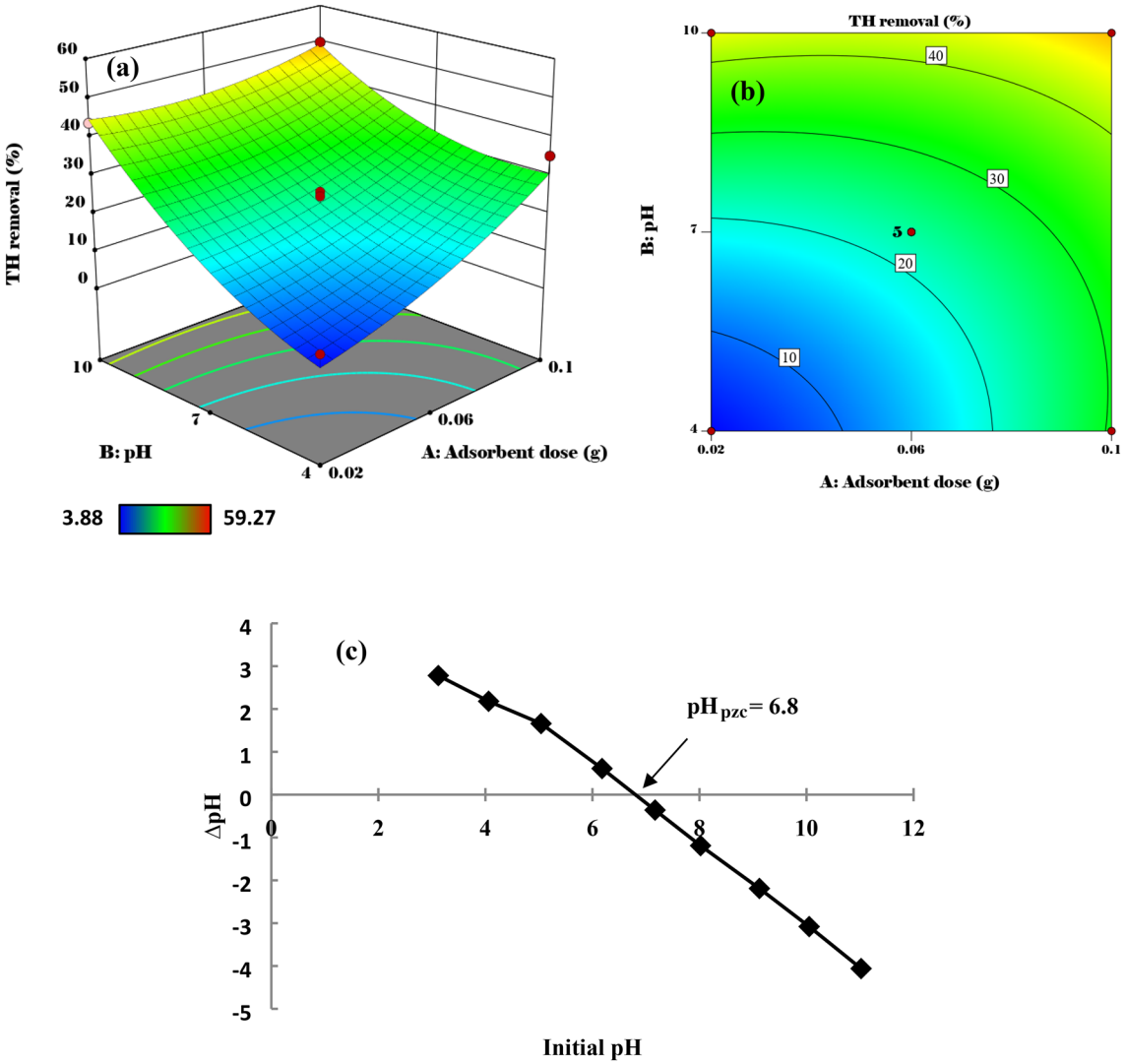


**Fig. 6** **a** 3D response surface plot, **b** 2D contour plot of TH removal showing interaction between adsorbent dose and pH, and **c** $pH_{PZC}$ of Ch-Glu/AC composite

## Significant Interactions on the TH Dye Removal

The interaction effect between the adsorbent dose and solution pH is statistically significant on the removal of the TH dye. Meanwhile, the other parameters (temperature = 40 °C, time = 150 min) are kept constant. The 3D response surfaces and 2D contour plots of the interaction between pH and adsorbent dose are given in Fig. 6a and b, respectively. It can be observed clearly from Fig. 6a and b that the TH dye removal (%) increased by raising the solution pH from 4 to 10. The $pH_{pzc}$ of the Ch-Glu/AC is 6.8 as presented in Fig. 6c. This result reveals that the Ch-Glu/AC surface can acquire a positive charge at $pH < pH_{pzc}$. Accordingly, the surface charge of Ch-Glu/AC is negative at pH 10 ($pH > pH_{pzc}$), indicating the favorable active sites of Ch-Glu/AC for the adsorption of organic dyes such as TH that contain cation groups. As a result, favorable electrostatic attractions can occur between the positive charge of Ch-Glu/AC with negative charge and the TH dye cation group, as seen in Eq. 5:

$$\mathrm{Ch-Glu/AC-O^- + TH^+ \leftrightarrow Ch-Glu/AC-O^- \cdots \cdots^+ TH} \quad (5)$$

The interaction between adsorbent dose and contact time on the removal of the TH dye is statistically significant. Meanwhile, the other parameters (pH 7 and temperature = 40 °C) are kept constant. The 3D response surfaces and 2D contour plots of the interaction between adsorbent dose and time are given in Fig. 7a and b, respectively. It can be concluded from Fig. 7a and b that the TH dye

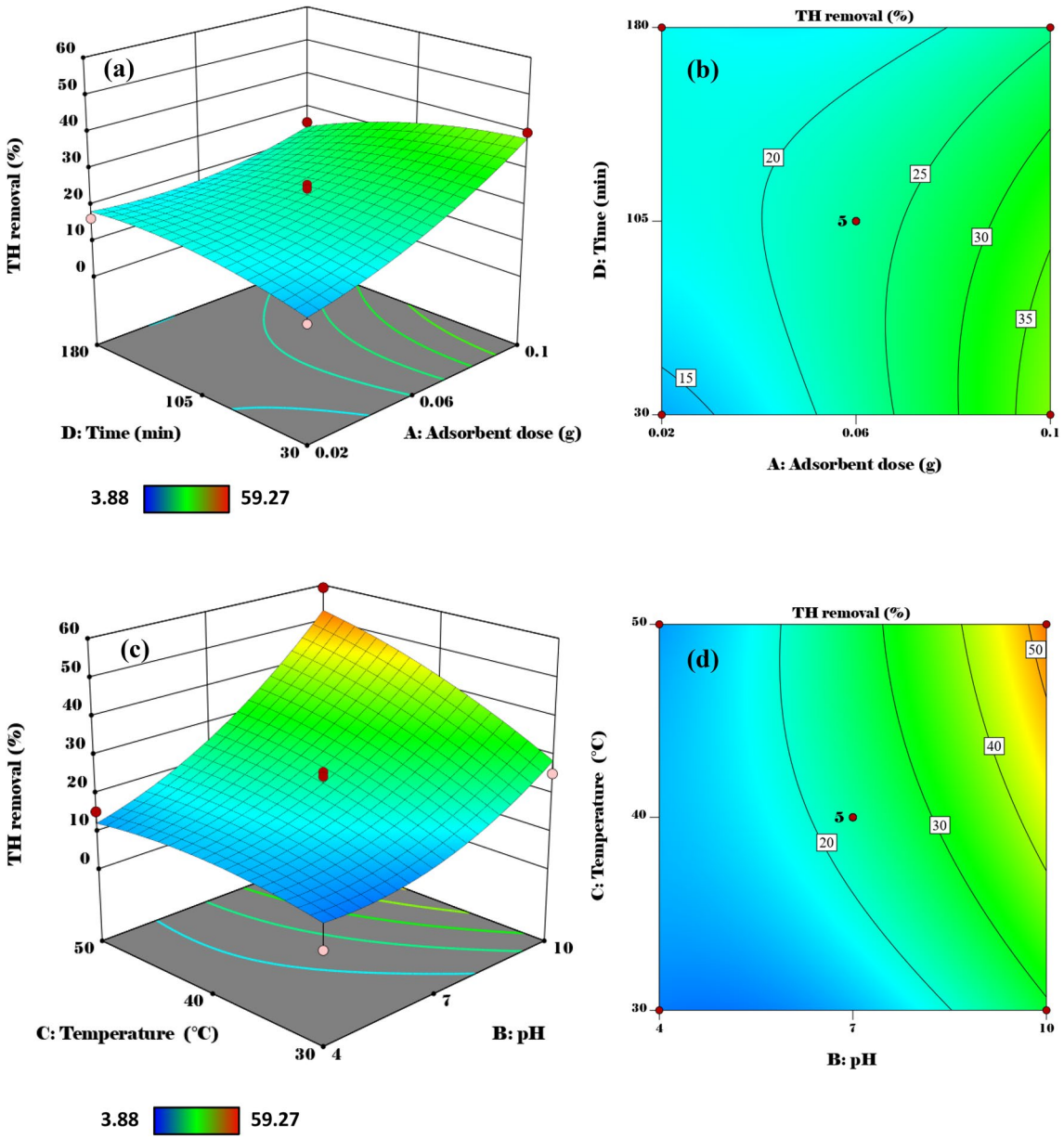


**Fig. 7** **a** 3D response surface plot, **b** 2D contour plot of TH removal showing interaction between adsorbent dose and time, **c** 3D response surface plot, and **d** 2D contour plot of TH removal showing interaction between temperature and pH

removal increased with greater adsorbent dose from 0.02 to 0.1 g, consistent with an increase in surface area and the number of active adsorption sites.

The interaction effect between the solution pH and temperature is also statistically significant on the removal of the TH dye. Meanwhile, the other parameters (adsorbent dose = 0.06 g and time = 105 min) are held constant. The 3D response surfaces and 2D contour plots of the interaction between solution pH and temperature are given in Fig. 7c and d, respectively. It is noticeable from Fig. 7c and d, a slight increase in the TH dye removal (%) occurs with increasing temperature up 50 °C. This trend between temperature and the incremental adsorption of dyes on the surface of Ch-Glu/AC reveals that the adsorption process is endothermic.

## Equilibrium Adsorption Study

The effect of contact time on the adsorption of dye molecules onto the surface of Ch-Glu/AC at different dye initial concentration (10, 20, 30, 40, 50, 70 and 100 mg/L) was studied. As well, the other parameters such as adsorbent dose = 0.07 g/100 mL, solution pH 10, temperature = 50 °C were held constant. The profiles of the adsorption capacity

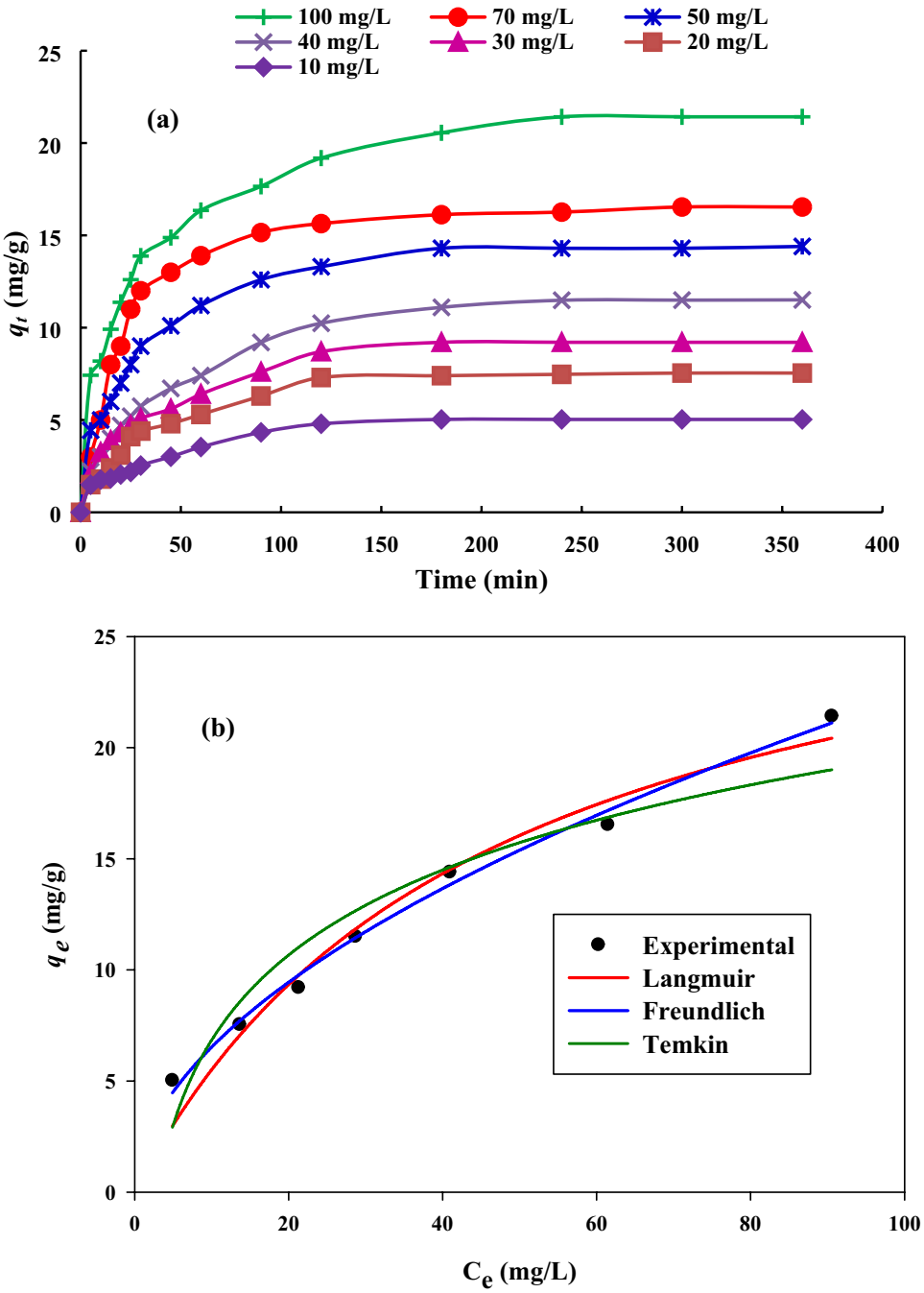


**Fig. 8** **a** Effect of the contact time on TH adsorption at different initial concentrations, and **b** adsorption isotherms of TH dye by Ch-Glu/AC composite (adsorbent dose = 0.06 g, pH of solution = 10, temperature = 323 K, agitation speed = 100 rpm and volume of solution = 100 mL)

($q_t$; mg/g) of Ch-Glu/AC versus time (min) at variable initial concentration of TH dye are shown in Fig. 8a. In Fig. 8a, the adsorption capacity of Ch-Glu/AC towards TH dye molecules increased from 5 to 21.4 mg/g as the dye concentration increased from 10 to 100 mg/L. This result is attributed to the diffusion of dye molecules in the pores of adsorbent is enhanced at higher dye concentrations [33].

## Kinetics of Adsorption Study

In order to explore the mechanism of the TH dye adsorption process on the surface of Ch-Glu/AC, two kinetic models were tested: the pseudo-first-order (PFO) and pseudo-second-order (PSO) models. The PFO [34] and PSO [35] models in non-linear forms are detailed by Eqs. (6) and (7) respectively:

**Table 5** PFO and PSO kinetic parameters for TH dye adsorption by Ch-Glu/AC composite

| Concentration (mg/L) | $q_{e\,exp}$. (mg/g) | PFO | | | | | |
|---|---|---|---|---|---|---|---|
| | | $q_{e\,cal}$ (mg/g) | $k_1$ (1/min) | $R^2$ | $q_{e\,cal}$ (mg/g) | $k_2 \times 10^{-2}$ (g/mg min) | $R^2$ |
| 10 | 5.0 | 4.97 | 0.025 | 0.96 | 5.6 | 0.557 | 0.95 |
| 20 | 7.5 | 7.41 | 0.026 | 0.98 | 8.5 | 0.372 | 0.94 |
| 30 | 9.2 | 8.94 | 0.028 | 0.97 | 10.1 | 0.362 | 0.93 |
| 40 | 11.5 | 11.21 | 0.023 | 0.98 | 12.9 | 0.211 | 0.98 |
| 50 | 14.4 | 13.8 | 0.034 | 0.95 | 15.4 | 0.298 | 0.97 |
| 70 | 16.5 | 16.0 | 0.041 | 0.98 | 17.8 | 0.305 | 0.96 |
| 100 | 21.4 | 20.0 | 0.040 | 0.90 | 22.2 | 0.248 | 0.94 |

**Table 6** Langmuir, Freundlich, and Temkin isotherm models for TH dye adsorption by Ch-Glu/AC composite at 323 K

| Adsorption isotherm | Parameter | Value |
|---|---|---|
| Langmuir | $q_m$ (mg/g) | 30.8 |
| | $K_a$ (L/mg) | 0.02 |
| | $R^2$ | 0.96 |
| Freundlich | $K_f$ (mg/g) (L/mg)$^{1/n}$ | 1.9 |
| | $n$ | 1.8 |
| | $R^2$ | 0.99 |
| Temkin | $K_T$ (L/mg) | 1.06 |
| | $b_T$ (J/mol) | 486.3 |
| | $R^2$ | 0.92 |

$$q_t = q_e(1 - \exp^{-k_1 t}) \tag{6}$$

$$q_t = \frac{q_e^2 k_2 t}{1 + q_e k_2 t} \tag{7}$$

$q_t$ (mg/g) and $q_e$ (mg/g) represent the amount of TH dye uptake by Ch-Glu/AC at time (t), and at equilibrium, respectively. $k_1$ (1/min), and $k_2$ (g/mg min) indicate rate constants of kinetic models.

The parameters of kinetic models are listed in Table 5. Accordingly, the TH dye uptake on the surface of Ch-Glu/AC was found to obey the PFO model because of the greater $R^2$ values, in addition to the calculated $q_e$ ($q_{e,cal}$) values by the PFO model. The PFO estimates are close to the experimental $q_e$ ($q_{e,exp}$) values, as compared to the calculated $q_e$ ($q_{e,cal}$) values by the PSO model in Table 5. This finding reveals that the TH dye uptake by Ch-Glu/AC is dominated by physical adsorption [36].

## Equilibrium Adsorption Isotherm Results

Equilibrium isotherms provide impactful parameters to investigate and describe the affinity of the Ch-Glu/AC towards TH molecules. Several well-known isotherm models (Langmuir, Freundlich, and Temkin) were evaluated to explicate the TH dye-Ch-Glu/AC interaction. The non-linear Langmuir, Freundlich, and Temkin isotherm models [37–39] are given in Eqs. (8), (9), and (10), respectively, as follows:

$$q_e = \frac{q_{\max} K_a C_e}{1 + K_a C_e} \tag{8}$$

$$q_e = K_f C_e^{1/n} \tag{9}$$

**Table 7** Comparison of the adsorption capacity of cationic dyes by various adsorbents

| Adsorbent | Dye | $q_m$ (mg/g) | References |
|---|---|---|---|
| Ch-Glu/AC composite | Thionine | 30.8 | This study |
| Mesoporous Iraqi red kaolin clay | Methylene blue | 240.4 | [33] |
| Modified coal fly ash with sulfonic acid | Malachite green | 233.3 | [41] |
| Commercial coconut shell activated carbon | Methylene blue | 149.25 | [42] |
| Mesoporous-activated carbon | Methylene blue | 143.53 | [43] |
| Magnetite nanoparticles loaded tea waste | Thionine | 128.21 | [44] |
| Crosslinked chitosan/activated charcoal composite | Thionine | 60.9 | [45] |
| Acid-functionalized biomass | Methylene blue | 50.6 | [46] |
| Magnetic multi-wall carbon nanotubes | Thionine | 36.63 | [47] |
| $H_2SO_4$ magnetic chitosan nanocomposite | Methylene blue | 20.41 | [48] |

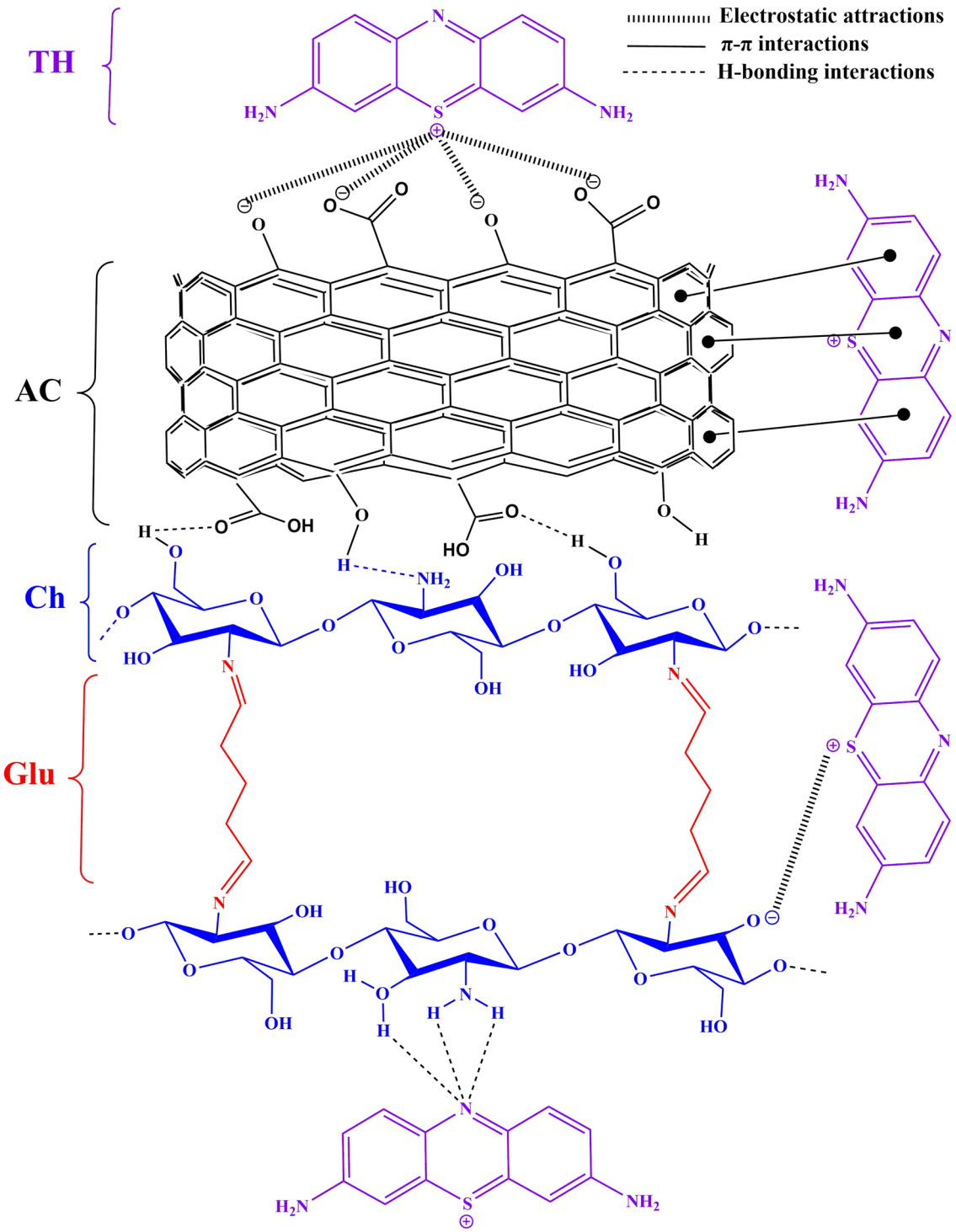


**Fig. 9** Illustration of the possible interactions between surface of Ch-Glu/AC composite and TH dye that include electrostatic, hydrogen bonding, and π-π stacking

$$q_e = \frac{RT}{b_T}\ln(K_T C_e) \quad (10)$$

$q_e$ (mg/g) is adsorption capacity of Ch-Glu/AC, $C_e$ (mg/L) is the residual amount of TH dye after adsorption at equilibrium, and $q_m$ (mg/g) is the saturated TH dye uptake of the monolayer. $K_a$ (L/mg), $K_f$ (mg/g) (L/mg)$^{1/n}$, and $K_T$ (L/mg) are constants of isotherms models. $n$ and $b_T$ (J/mol) represents adsorption intensity and heat of adsorption, respectively. $T$ (K) is the temperature, and $R$ (8.314 J/mol K) is the gas constant. The non-linear curves and parameters of isotherms are given in Fig. 8b and Table 6, respectively. It was found from $R^2$ (Table 6) that the adsorption of TH dye on the Ch-Glu/AC surface is described by the Freundlich isotherm, signifying the adsorption of TH dye adopted a multilayer adsorption profile onto the heterogeneous adsorbent surface [40]. The $q_m$ of Ch-Glu/AC for TH dye is 30.8 mg/g at 50 °C. Table 7 shows a comparison the $q_m$ of Ch-Glu/AC with other materials utilized for removal of cationic dyes. The results in Table 7 reveal that Ch-Glu/AC is a promising and efficient adsorbent to remove of TH dyes from water.

### Mechanism of TH Dye Adsorption on Ch-Glu/AC Surface

Various interactions are possible for capturing TH dye molecules on the Ch-Glu/AC surface as shown in Fig. 9. Electrostatic attraction is one of the significant interactions that occur between the TH dye cation with the negatively surface charged functional groups available on the surface of Ch-Glu/AC. Another significant interaction is hydrogen bonding between donor hydrogen sites of the Ch-Glu/AC surface with oxygen and nitrogen of the TH dye molecule. As well, π–π and cation–π interactions occur between the hexagonal skeleton of the Ch-Glu/AC composite and the aromatic ring of the TH dye. Similar conclusions have been reported for the uptake of cationic dyes by such composite Ch-AC derivatives [49, 50].

## Conclusion

A composite Ch-Glu/AC was successfully prepared by direct loading of AC with a Ch biopolymer, followed by a cross-linking reaction with Glu to yield an effective adsorbent for the removal of TH dye from aqueous solution. The optimum conditions of TH dye adsorption was obtained at a solution pH 10, adsorbent dose (0.06 g/L), and temperature (50 °C), where the $q_m$ value of Ch-Glu/AC for the dye was 30.8 mg/g. The experimental results reveal that the TH dye adsorption is influenced by physical adsorption on the heterogeneous surface of Ch-Glu/AC, attributed to electrostatic interactions such as π–π interactions, and H-bonding. The results reveal the feasibility of AC and cross-linked chitosan as a low-cost composite with potential utility as a suitable adsorbent for the uptake of cationic dyes, in parallel agreement with relevant chitosan-biomass composites reported elsewhere [51].

**Acknowledgements** The authors acknowledge the Ministry of Education (MOE) Malaysia, for funding this research project under Fundamental Research Grant Scheme (FRGS): FRGS/1/2019/STG01/UiTM/02/3, No. Fail RMC: 600-IRMI/FRGS 5/3 (340/2019). The authors would also like to thank the Researchers Supporting Project No. (RSP-2020/138) King Saud University, Riyadh, Saudi Arabia.

## References

1. Madrakian T, Afkhami A, Ahmadi M (2012) Adsorption and kinetic studies of seven different organic dyes onto magnetite nanoparticles loaded tea waste and removal of them from wastewater samples. Spectrochim Acta A 99:102–109
2. Acar ET, Ortaboy S, Atun G (2015) Adsorptive removal of thiazine dyes from aqueous solutions by oil shale and its oil processing residues: characterization, equilibrium, kinetics and modeling studies. Chem Eng J 276:340–348
3. Nidheesh PV, Zhou M, Oturan MA (2018) An overview on the removal of synthetic dyes from water by electrochemical advanced oxidation processes. Chemosphere 197:210–227
4. Moradnia F, Fardood ST, Ramazani A, Gupta VK (2020) Green synthesis of recyclable $MgFeCrO_4$ spinel nanoparticles for rapid photodegradation of direct black 122 dye. J Photochem Photobiol A 392:112433
5. Hassan MM, Carr CM (2018) A critical review on recent advancements of the removal of reactive dyes from dyehouse effluent by ion-exchange adsorbents. Chemosphere 209:201–219
6. Abdulhameed AS, Jawad AH, Mohammad AT (2020) Statistical optimization for dye removal from aqueous solution by cross-linked chitosan composite. Sci Lett 14(2):1–14
7. Beluci NDCL, Mateus GAP, Miyashiro CS, Homem NC, Gomes RG, Fagundes-Klen MR, Vieira AMS (2019) Hybrid treatment of coagulation/flocculation process followed by ultrafiltration in $TIO_2$-modified membranes to improve the removal of reactive black 5 dye. Sci Total Environ 664:222–229
8. Malek NNA, Jawad AH, Abdulhameed AS, Ismail K, Hameed BH (2020) New magnetic Schiff's base-chitosan-glyoxal/fly ash/$Fe_3O_4$ biocomposite for the removal of anionic azo dye: an optimized process. Int J Biol Macromol 146:530–539
9. Abdulhameed AS, Mohammad AT, Jawad AH (2019) Modeling and mechanism of reactive orange 16 dye adsorption by chitosan-glyoxal/ $TiO_2$ nanocomposite: application of response surface methodology. Desalin Water Treat 164:346–360
10. Wu J, Cheng X, Yang G (2019) Preparation of nanochitin-contained magnetic chitosan microfibers via continuous injection gelation method for removal of Ni (II) ion from aqueous solution. Int J Biol Macromol 125:404–413
11. Abdulhameed AS, Jawad AH, Mohammad AT (2019) Synthesis of chitosan-ethylene glycol diglycidyl ether/$TiO_2$ nanoparticles for adsorption of reactive orange 16 dye using a response surface methodology approach. Bioresour Technol 293:122071
12. Naskar S, Sharma S, Koutsu K (2019) Chitosan-based nanoparticles: an overview of biomedical applications and its preparation. J Drug Deliv Sci Technol 49:66–81
13. Sharififard H, Rezvanpanah E, Rad SH (2018) A novel natural chitosan/activated carbon/iron bio-nanocomposite: sonochemical synthesis, characterization, and application for cadmium

removal in batch and continuous adsorption process. Bioresour Technol 270:562–569
14. Jawad AH, Malek NNA, Abdulhameed AS, Razuan R (2020) Synthesis of magnetic chitosan-Fly Ash/$Fe_3O_4$ composite for adsorption of reactive orange 16 dye: optimization by Box-Behnken design. J Polym Environ 28:1068–1082
15. Mohammad AT, Abdulhameed AS, Jawad AH (2019) Box-Behnken design to optimize the synthesis of new crosslinked chitosan-glyoxal/$TiO_2$ nanocomposite: methyl orange adsorption and mechanism studies. Int J Biol Macromol 129:98–109
16. Guo M, Wang J, Wang C, Strong PJ, Jiang P, Ok YS, Wang H (2019) Carbon nanotube-grafted chitosan and its adsorption capacity for phenol in aqueous solution. Sci Total Environ 682:340–347
17. Jóźwiak T, Filipkowska U, Szymczyk P, Rodziewicz J, Mielcarek A (2017) Effect of ionic and covalent crosslinking agents on properties of chitosan beads and sorption effectiveness of Reactive Black 5 dye. React Funct Polym 114:58–74
18. Thomas TD (2008) The role of activated charcoal in plant tissue culture. Biotechnol Adv 26(6):618–631
19. Roy S, Das P, Sengupta S, Manna S (2017) Calcium impregnated activated charcoal: optimization and efficiency for the treatment of fluoride containing solution in batch and fixed bed reactor. Process Saf Environ 109:18–29
20. Pinho MT, Silva AM, Fathy NA, Attia AA, Gomes HT, Faria JL (2015) Activated carbon xerogel–chitosan composite materials for catalytic wet peroxide oxidation under intensified process conditions. J Environ Chem Eng 3(2):1243–1251
21. Danalıoğlu ST, Bayazit ŞS, Kuyumcu ÖK, Salam MA (2017) Efficient removal of antibiotics by a novel magnetic adsorbent: magnetic activated carbon/chitosan (MACC) nanocomposite. J Mol Liq 240:589–596
22. Wróbel-Iwaniec I, Díez N, Gryglewicz G (2015) Chitosan-based highly activated carbons for hydrogen storage. Int J Hydrogen Energy 40(17):5788–5796
23. Keramati M, Ghoreyshi AA (2014) Improving $CO_2$ adsorption onto activated carbon through functionalization by chitosan and triethylenetetramine. Physica E 57:161–168
24. Tang C, Hu D, Cao Q, Yan W, Xing B (2017) Silver nanoparticles-loaded activated carbon fibers using chitosan as binding agent: preparation, mechanism, and their antibacterial activity. Appl Surf Sci 394:457–465
25. Wang L, Wang Y, Li A, Yang Y, Wang J, Zhao H, Qi T (2014) Electrocatalysis of carbon black-or chitosan-functionalized activated carbon nanotubes-supported Pd with a small amount of $La_2O_3$ towards methanol oxidation in alkaline media. Int J Hydrogen Energy 39(27):14730–14738
26. Dalvand A, Nabizadeh R, Ganjali MR, Khoobi M, Nazmara S, Mahvi AH (2016) Modeling of Reactive Blue 19 azo dye removal from colored textile wastewater using L-arginine-functionalized $Fe_3O_4$ nanoparticles: optimization, reusability, kinetic and equilibrium studies. J Magn Mater 404:179–189
27. Sing KS (1985) Reporting physisorption data for gas/solid systems with special reference to the determination of surface area and porosity, (Recommendations 1984). Pure Appl Chem 57:603–619
28. Ahmed MJ, Okoye PU, Hummadi EH, Hameed BH (2019) High-performance porous biochar from the pyrolysis of natural and renewable seaweed (*Gelidiella acerosa*) and its application for the adsorption of methylene blue. Bioresour Technol 278:159–164
29. Jawad AH, Mubarak NSA, Abdulhameed AS (2020) Tunable Schiff's base-cross-linked chitosan composite for the removal of reactive red 120 dye: adsorption and mechanism study. Int J Biol Macromol 142:732–741
30. Barpanda P, Fanchini G, Amatucci GG (2011) Structure, surface morphology and electrochemical properties of brominated activated carbons. Carbon 49:2538–2548
31. Mohammed IA, Jawad AH, Abdulhameed AS, Mastulia MS (2020) Physicochemical modification of chitosan with fly ash and tripolyphosphate for removal of reactive red 120 dye: statistical optimization and mechanism study. Int J Biol Macromol 161:503–513
32. Moghaddam AZ, Ghiamati E, Pourashuri A, Allahresani A (2018) Modified nickel ferrite nanocomposite/functionalized chitosan as a novel adsorbent for the removal of acidic dyes. Int J Biol Macromol 120:1714–1725
33. Jawad AH, Abdulhameed AS (2020) Mesoporous Iraqi red kaolin clay as an efficient adsorbent for methylene blue dye: adsorption kinetic, isotherm and mechanism study. Surf Interface 18:100422
34. Lagergren S (1898) Zur theorie der sogenannten adsorption geloster stoffe. Vet Akad Handl 24:1–39
35. Ho YS, McKay G (1998) Sorption of dye from aqueous solution by peat. Chem Eng J 70:115–124
36. Zou X, Zhang H, Chen T, Li H, Meng C, Xia Y, Guo J (2019) Preparation and characterization of polyacrylamide/sodium alginate microspheres and its adsorption of MB dye. Colloids Surf A 567:184–192
37. Langmuir I (1918) The adsorption of gases on plane surfaces of glass, mica and platinum. J Am Chem Soc 40:1361–1403
38. Frenudlich HMF (1906) Over the adsorption in solution. J Phys Chem 57:385–471
39. Temkin MI (1940) Kinetics of ammonia synthesis on promoted iron catalysts. Acta Physiochim URSS 12:327–356
40. Abdulhameed AS, Mohammad AT, Jawad AH (2019) Application of response surface methodology for enhanced synthesis of chitosan tripolyphosphate/$TiO_2$ nanocomposite and adsorption of reactive orange 16 dye. J Clean Prod 232:43–56
41. Dash S, Chaudhuri H, Gupta R, Nair UG (2018) Adsorption study of modified coal fly ash with sulfonic acid as a potential adsorbent for the removal of toxic reactive dyes from aqueous solution: kinetics and thermodynamics. J Environ Chem Eng 6(5):5897–5905
42. Rashid RA, Ishak MAM, Hello KM (2018) Adsorptive removal of methylene blue by commercial coconut shell activated carbon. Sci Lett 12:27–97
43. Marrakchi F, Ahmed MJ, Khanday WA, Asif M, Hameed BH (2017) Mesoporous-activated carbon prepared from chitosan flakes via single-step sodium hydroxide activation for the adsorption of methylene blue. Int J Biol Macromol 98:233–239
44. Madrakian T, Afkhami A, Ahmadi M (2012) Adsorption and kinetic studies of seven different organic dyes onto magnetite nanoparticles loaded tea waste and removal of them from wastewater samples. Spectrochim Acta A Mol Biomol Spectrosc 99:102–109
45. Jawad AH, Abdulhameed AS, Mastuli MS (2020) Mesoporous crosslinked chitosan-activated charcoal composite for the removal of thionine cationic dye: comprehensive adsorption and mechanism study. J Polym Environ 28(3):1095–1105
46. Jawad AH, Abdulhameed AS, Mastuli MS (2020) Acid-factionalized biomass material for methylene blue dye removal: a comprehensive adsorption and mechanism study. J Taibah Univ Sci 14(1):305–313
47. Madrakian T, Afkhami A, Ahmadi M, Bagheri H (2011) Removal of some cationic dyes from aqueous solutions using magnetic-modified multi-walled carbon nanotubes. J Hazard Mater 196:109–114
48. Ishmaturrahmi R, Mustafa I (2019) Methylene blue removal from water using $H_2SO_4$ crosslinked magnetic chitosan nanocomposite beads. Microchem J 144:397–402
49. Karaer H, Kaya I (2016) Synthesis, characterization of magnetic chitosan/active charcoal composite and using at the adsorption of methylene blue and reactive blue4. Microporous Mesoporous Mater 232:26–38

50. Yan M, Huang W, Li Z (2019) Chitosan cross-linked graphene oxide/lignosulfonate composite aerogel for enhanced adsorption of methylene blue in water. Int J Biol Macromol 136:927–935
51. Mohamed MH, Udoetok IA, Wilson LD (2020) Animal biopolymer-plant biomass composites: synergism and improved sorption efficiency. J Compos Sci 4(1):15